Propagation of the 12 May 1997 interplanetary coronal mass ejection in evolving solar wind structures

D. Odstrcil[1]

Cooperative Institute for Research in Environmental Sciences, University of Colorado, Boulder, Colorado, USA

Space Environment Center, Atmospheric Administration, Boulder, Colorado, USA

V. J. Pizzo

Space Environment Center, National Oceanic and Atmospheric Administration, Boulder, Colorado, USA

C. N. Arge

Space Vehicles Directorate, Air Force Research Laboratory, Hanscom Air Force Base, Massachusetts, USA

Received 15 August 2004; revised 8 October 2004; accepted 6 December 2004; published 26 February 2005.

[1] Recently, we simulated the 12 May 1997 coronal mass ejection (CME) event with a numerical three-dimensional magnetohydrodynamic model (Odstrcil et al., 2004), in which the background solar wind was determined from the Science Applications International Corporation (SAIC) coronal model (Riley et al., 2001) and the transient disturbance was determined from the cone model (Zhao et al., 2002). Although we reproduced with some fidelity the arrival of the shock and interplanetary CME at Earth, detailed analysis of the simulations showed a poorly defined shock and discrepancies in the standoff distance between the shock and the driving ejecta and in the inclination of the shock with respect to the Sun-Earth line. In this paper, we investigate these problems in more detail. First, we use an alternative coronal outflow model, the so-called Wang-Sheeley-Arge-Mount Wilson Observatory (WSA-MWO) model (Arge and Pizzo, 2000; Arge et al., 2002; Arge et al., 2004), to assess the effect of using synoptic, full rotation coronal maps that differ in method of preparation. Second, we investigate how differences in the presumed evolution of the coronal stream structure affect the propagation of the disturbance. We incorporate two time-dependent boundary conditions for the ambient solar wind as determined by the WSA model, one derived from pseudo daily updated maps and one derived from artificially modified full rotation maps. Numerical results from these different scenarios are compared with solar wind observations at Earth. We find that heliospheric simulations with the SAIC and WSA full rotation models provide qualitatively similar parameters of the background solar wind and transient disturbances at Earth. Improved agreement with the observations is achieved by artificially modified maps that simulate the rapid displacement of the coronal hole boundary after the CME eruption. We also consider how multipoint temporal profiles of solar wind parameters and multiperspective synthetic white light images emulating upcoming STEREO spacecraft observations might be used to differentiate between different event scenarios.

Citation: Odstrcil, D., V. J. Pizzo, and C. N. Arge (2005), Propagation of the 12 May 1997 interplanetary coronal mass ejection in evolving solar wind structures, *J. Geophys. Res.*, *110*, A02106, doi:10.1029/2004JA010745.

1. Introduction

[2] Solar and heliospheric background conditions for the 12 May 1997 coronal mass ejection (CME) event were undisturbed, which facilitates analysis and modeling [*Webb et al.*, 2000]. Recently, we applied a numerical three-dimensional (3-D) magnetohydrodynamic (MHD) model to simulate this event [*Odstrcil et al.*, 2004, hereinafter referred to as paper 1]. The ambient solar wind parameters were derived from the Science Applications International Corporation (SAIC) source-surface coronal model [*Riley et al.*, 2001] utilizing photospheric magnetic field observations from the Kitt Peak National Observatory (this coronal model is referred to here as the SAIC-KPNO model). The interplanetary CME (ICME) parameters were derived by

[1]On leave from Astronomical Institute, Ondřejov, Czech Republic.

0148-0227/05/2004JA010745$09.00

geometrical and kinematic fitting (the so-called cone model) of Solar and Heliospheric Observatory (SOHO)/Large Angle and Spectrometric Coronograph (LASCO) observations [*Zhao et al.*, 2002].

[3] That model reproduced with some fidelity the arrival of an interplanetary shock and ICME and also roughly reproduced the shock strength, solar wind parameters, and interplanetary magnetic field (IMF) strength and orientation in the sheath region between the shock and ejected plasma cloud (see paper 1). Further, it was found that relatively small scale structures ($\approx 10^\circ$ in the heliocentric system) may play an important role in the interplanetary evolution of transient disturbances. Finally, we also produced from that simulation synthetic white light images of the event that give a sense of the observations that will be obtained by the upcoming STEREO mission [*Odstrcil et al.*, 2003].

[4] However, detailed analysis of the simulations shows a poorly defined interplanetary shock and discrepancies in the standoff distance between the shock and the driving ejecta and in the inclination of the shock with respect to the Sun-Earth line. We suggested that these discrepancies may be caused by interaction of the shock with the leading edge of the preexisting ambient high-speed stream in a similar manner as presented by *Odstrcil and Pizzo* [1999a].

[5] In this paper, we investigate modeling of the 12 May 1997 event in more detail. First, we use an alternative coronal outflow model, the so-called –Mount Wilson Observatory (WSA-MWO) model [*Arge and Pizzo*, 2000; *Arge et al.*, 2002; *Arge et al.*, 2004], to assess the effect of using synoptic, full rotation coronal maps that differ in method of preparation. Then, we apply pseudo daily updated maps and artificially modified maps to simulate the temporal variation of the ambient solar wind and rapid displacement of the streamer boundary, respectively. We compare numerical results from these different scenarios with Wind spacecraft observations at Earth, and we also provide multipoint temporal profiles of plasma parameters and multiperspective synthetic white light images as might be seen from the future STEREO spacecraft.

2. Numerical Simulations

[6] Here we present a brief summary of the new computational configuration and how it differs from the previous work. Details are given in paper 1 and references therein.

2.1. Numerical Model

[7] We use the same physical and numerical parameters for the 3-D MHD heliospheric code as in paper 1. The grid resolution is the same in latitude and longitude but slightly finer in radius. The computational region has $512 \times 60 \times 180$ grid points (corresponding to r, θ, and φ, respectively) and spans from 0.1 to 1.7 AU (instead of $256 \times 120 \times 180$ from 0.14 to 1.14 AU). The larger radial extent is necessary for proper computation of line-of-sight synthetic white light images presented in this paper.

2.2. Ambient Solar Wind

[8] The ambient solar wind parameters in the heliosphere are determined by values at the inner boundary. We use data from the National Oceanic and Atmospheric Administration/Space Environment Center repository of synoptic maps of magnetic field and velocity at 21.5 R_S [*Arge and Pizzo*, 2000]. These data are based on the coupled potential source-surface Schatten current sheet model [*Schatten*, 1971; *Wang and Sheeley*, 1995] as applied by *Arge et al.* [2002]. The empirical relationship used [e.g., *Arge et al.*, 2004] is a function of both the magnetic field expansion factor and the distance of a solar wind source region from the nearest coronal hole boundary. The coronal solution itself is determined by photospheric magnetic field observations from the Mount Wilson Solar Observatory. This coronal model is referenced here as the WSA-MWO model.

2.3. Transient Disturbances

[9] The cone model has been applied to characterize the expanding halo CME observed by the LASCO/C3 coronagraph on 12 May 1997 [*Zhao et al.*, 2002]. The best fit suggested an angular width of 50° and a central axis of the cone pointing to 3.0°N and 1.0°W. The CME was determined to be traveling at 650 km s^{-1} at 24 R_S (observed at 1415:05 UT) and was accelerating at $\sim$18.5 m s^{-2}. We estimate that visible edges of the halo CME reached a height of 21.5 R_S at 1400 UT with a speed of 650 km s^{-1}; that is, the leading edge of the assumed spherical ejecta reached that height at 1112 UT, and it took 5.6 hours to pass through that position. Note that these values are slightly different from those used previously in paper 1 because of the different inner boundary location used (i.e., 21.5 R_S here compared to 30 R_S in paper 1). Finally, we have specified here the input pulse as a spherical cloud passing through the inner boundary.

[10] For numerical computations we assume a spherical plasma cloud with the location, diameter, and velocity corresponding to the cone model parameters. Time-dependent conditions specify the cloud passing through the inner boundary, i.e., the launch of the simulated ICME into the background solar wind. We assume that the cloud is homogeneous with a uniform velocity corresponding to the estimated CME speed. Further, we assume the cloud's density (temperature) to be 4 times larger than (equal to) the mean values in the fast stream. Thus the plasma cloud has $\sim$4 times more pressure than the ambient fast wind. Note that the density values within the cloud are about as large as maximum values in the slow streamer belt at the inner boundary of the model.

3. Effects of Using an Alternative Coronal Model

[11] The SAIC-KPNO and WSA-MWO are different coronal models that utilize the photospheric magnetic field measured at different observatories. Thus they provide different background solar wind for heliospheric simulations of transient disturbances. We have taken this opportunity to verify results presented in paper 1 as well as to assess the consequences of using different coronal input models.

3.1. Full Rotation Maps

[12] Figure 1 shows the distribution of parameters at the heliospheric inner boundary for the undisturbed ambient solar wind (Figure 1, top) and the ambient solar wind with the input pulse (Figure 1, bottom). In general, the SAIC-

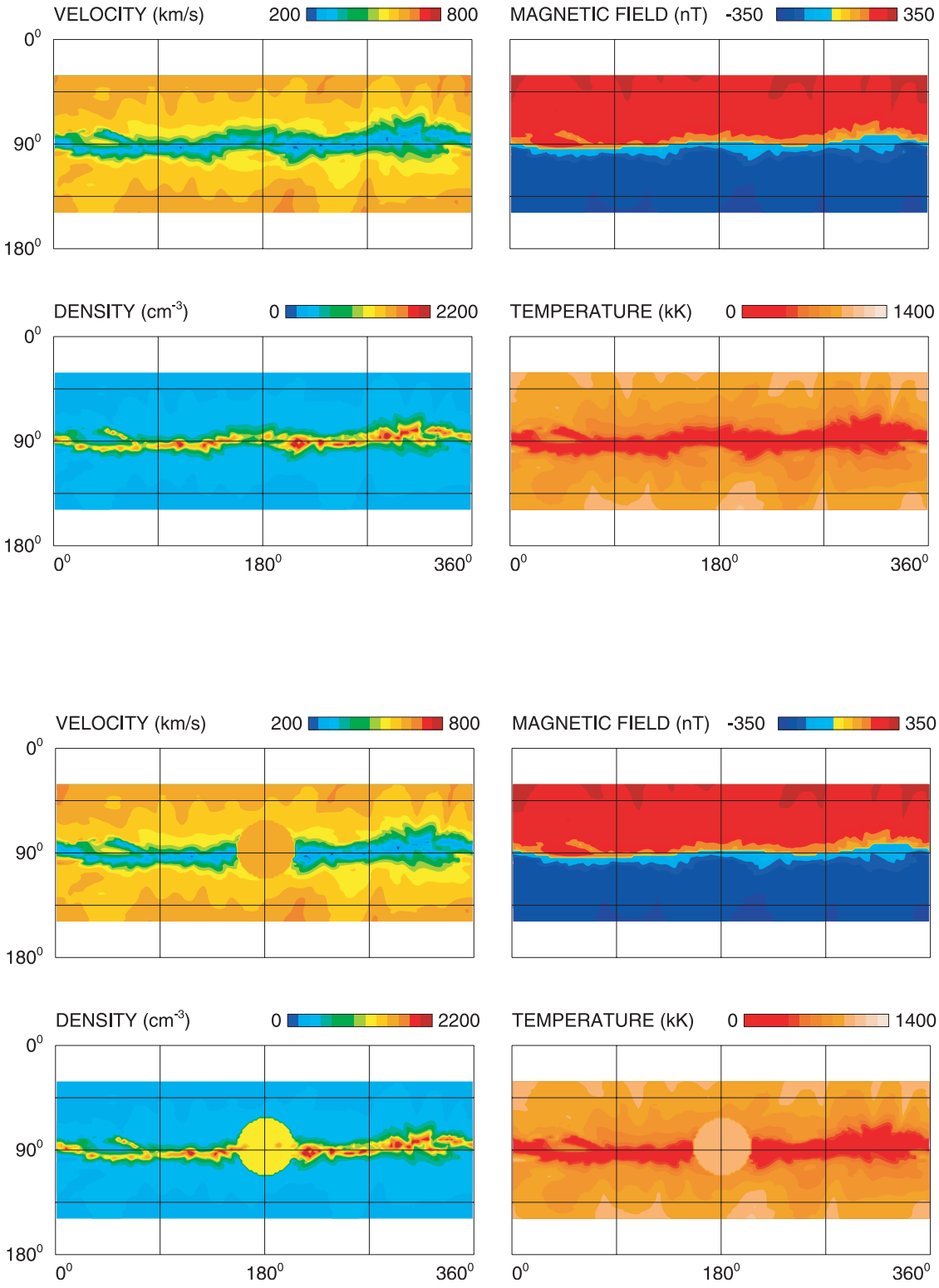

Figure 1. Distribution of solar wind parameters (outflow velocity, magnetic field strength, number density, and temperature) on the inner boundary (at 0.1 AU) for the –Mount Wilson Observatory (WSA-MWO) full rotation (FR) maps (top) without and (bottom) with introduction of the input pulse. The distribution of parameters is shown on 12 May 1997 at 1800 UT, i.e., at the time of maximum diameter of the spherical input pulse.

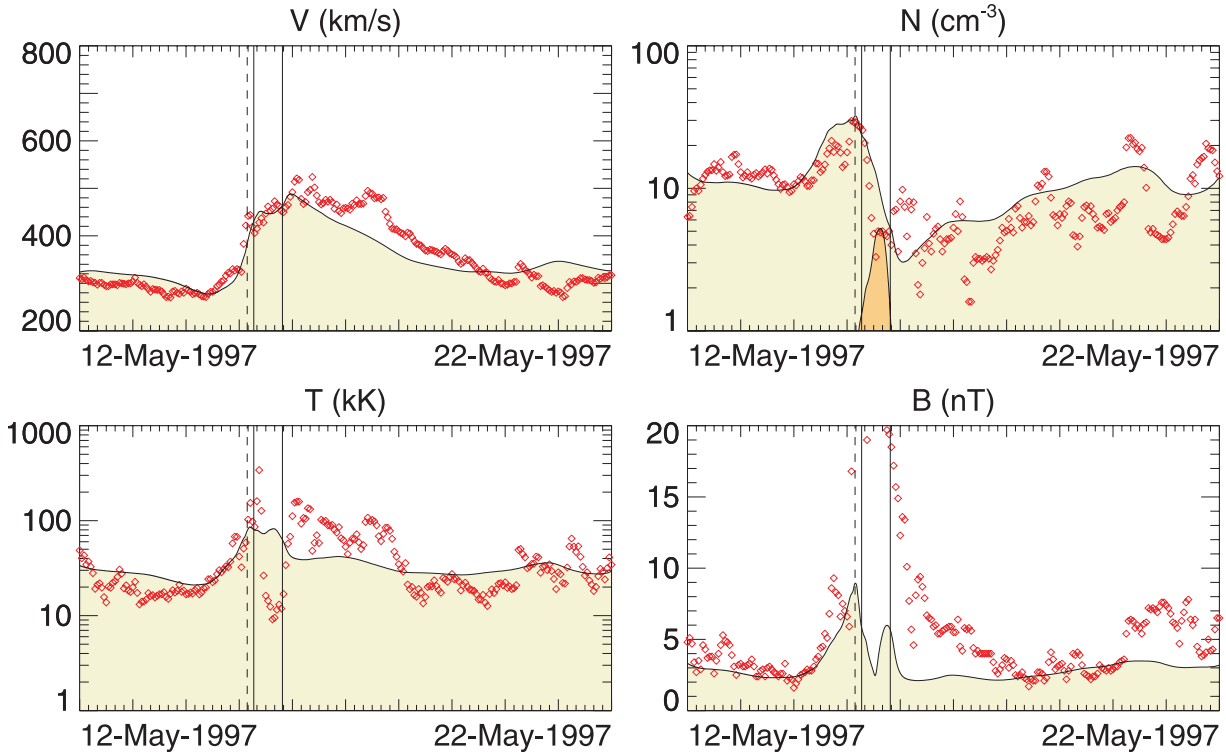

Figure 2. Evolution of solar wind parameters at Earth for the interplanetary coronal mass ejection (ICME) propagating in the background solar wind derived from the WSA-MWO-FR maps. Shown are the flow velocity, number density, temperature, and magnetic field strength. Results of the numerical simulation are shown by black solid lines with yellow shading. The observational data were obtained from the NASA National Space Science Data Center (available at http://nssdc.gsfc.nasa.gov/cohoweb/cw.html), and they are shown by red diamonds. The vertical solid lines indicate the extent of the simulated ICME material, and the black line with orange shading on the density plot shows the injected number density. The vertical dashed lines indicate the forward shock or compressive pressure wave.

KPNO and WSA-MWO models provide similar distributions of parameters at the inner boundary of the heliospheric computational model. These results were both derived using traditional line-of-sight photospheric magnetic field Carrington (or full rotation (FR)) synoptic maps. The SAIC-KPNO-FR model provides (see paper 1) faster, more homogeneous solar wind at higher latitudes and more speed contrast in fast streams emanating from a near-equatorial coronal hole than does the WSA-MWO-FR model. However, the heliospheric current sheet (HCS) has about the same configuration in both models, and the outflow parameters are similar near the ecliptic.

[13] Note that there is a small excursion of the fast stream from the southern coronal hole up to the solar equator near 180° longitude. This small-scale feature (obtained with the WSA-MWO-FR model) has less velocity contrast but is similar to the one described in paper 1 (obtained with the SAIC-KPNO-FR model). *Ivanov et al.* [2003] considered the low-latitude coronal hole as one of the sources of the near-Earth disturbance. *Arge et al.* [2004] investigated the stream structure and coronal sources of the solar wind during the 12 May 1997 CME and found that the northern active region associated with the CME did not play a role in the formation of the small southern coronal hole extension that produced the high-speed stream.

3.2. Evolution at Earth

[14] Figure 2 shows the evolution of the disturbed solar wind parameters at Earth. The numerical results show reasonable agreement with the parameters observed by the Wind spacecraft. Thus we can draw the same positive conclusion that we drew in paper 1 (see its Figure 5) that the ambient solar wind ahead of the transient disturbance and the shock arrival time are in agreement with observations (observed at 0115 UT and predicted at 0336 UT). Shock compression values and the rarefaction beyond the plasma cloud appear to also be consistent with observations. Thus, using either the SAIC-KPNO-FR or WSA-MWO-FR coronal maps, we have simulated heliospheric transient structures that are in global agreement with observations.

[15] However, upon closer inspection, heliospheric simulations produce profiles of the solar wind parameters at Earth that yield a poorly defined, smoothed interplanetary shock with a very small standoff distance from the driving ejecta. These artifacts are similar to those presented in paper 1 which used the SAIC-KPO-FR maps, and we analyze them with additional visualizations in section 3.3.

3.3. Heliospheric Interactions

[16] The initially fast ICME propagates into a corotating interaction region (CIR) that formed from the interaction between the fast, low-density flow and the southern coronal

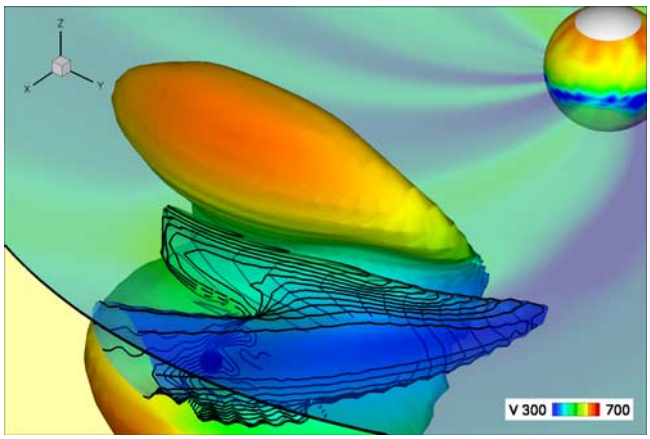

Figure 3. Visualization of an interplanetary disturbance on 15 May 1997 at 0000 UT for the ICME propagating in the background solar wind derived from the WSA-MWO-FR maps. The solar wind radial velocity is shown on the inner boundary (at 0.1 AU) and on the equatorial plane using a translucent color scale. The cloud is shown as an isosurface for the injected density at 6 cm^{-3}; the isosurface is colored according to the corresponding value of the solar wind velocity. The contours ahead of the cloud show an isosurface for the total density at 20 cm^{-3}. Both the injected and total density values are scaled by $(R_{AU}/r)^2$. The Earth's position is shown by a small blue sphere.

hole extension with the slow, dense streamer belt flow. The ICME is launched with an initial speed about the same as that of the fast flow but approximately twice the speed of the heliospheric streamer belt flow. This results in significant compression of the injected plasma as well as the formation of a shock in this region, which can be seen in Figure 3 as an arc-like high-density structure [see also *Odstrcil et al.*, 2003, Figure 7]. The SAIC-KPNO-FR wind produces larger latitudinal distortion of the ejected plasma cloud than the WSA-MWO-FR wind. However, both models lead to similar scenarios when the transient disturbances hit the Earth. The ejected material occupies a large volume, but its interaction with the background solar wind is the greatest near the equator where the dense slower stream is located.

[17] Figure 4 shows that the simulated ICME interacts with the moderate fast stream that results from the excursion of the southern coronal hole toward the helioequator. The transient disturbance propagates through the fast stream and later merges with its leading edge. This effect is facilitated by the systematic difference in characteristic speeds in fast and slow streams; the fast stream with higher temperature and lower density has faster characteristic speeds than the slow stream. Thus the compressive pressure waves are retarded by the colder and denser medium ahead, and the transient disturbance merges with the leading edge of the CIR. When the transient disturbances arrive at Earth, the interplanetary shock and ICME are already merged with the CIR and have acquired its inclination. Note also the formation of a forward and reverse, fast-mode MHD, transient shock pair structure and their gradual separation with the increasing heliospheric distance.

[18] *Odstrcil and Pizzo* [1999a] demonstrated that on occasions where the ejection lies in the tilted slow-speed flow structure in such a way that it is followed by higher-speed wind, the ejecta can appear at the leading edge of a high-speed stream. Such temporal profiles at 1 AU bear some similarity to the 12 May 1997 interplanetary event; however, in this instance the streamer belt lies in the equatorial plane with very little inclination. Thus fast solar wind can be observed behind the ICME either (1) when the ICME propagates in a local excursion of the polar coronal hole or (2) when a transient fast stream forms behind the ICME (e.g., caused by an opening or displacement of the coronal hole associated with the eruption). In the first case, there will be no significant interaction between the ICME and corotating streamer unless the excursion is significant. In the second case the ICME will propagate into an undisturbed slow streamer belt flow.

4. Effects of Evolving Solar Wind

[19] The simulations discussed in section 3 used the full rotation maps in which the background solar wind structure remains constant over a 27-day period. In both the SAIC

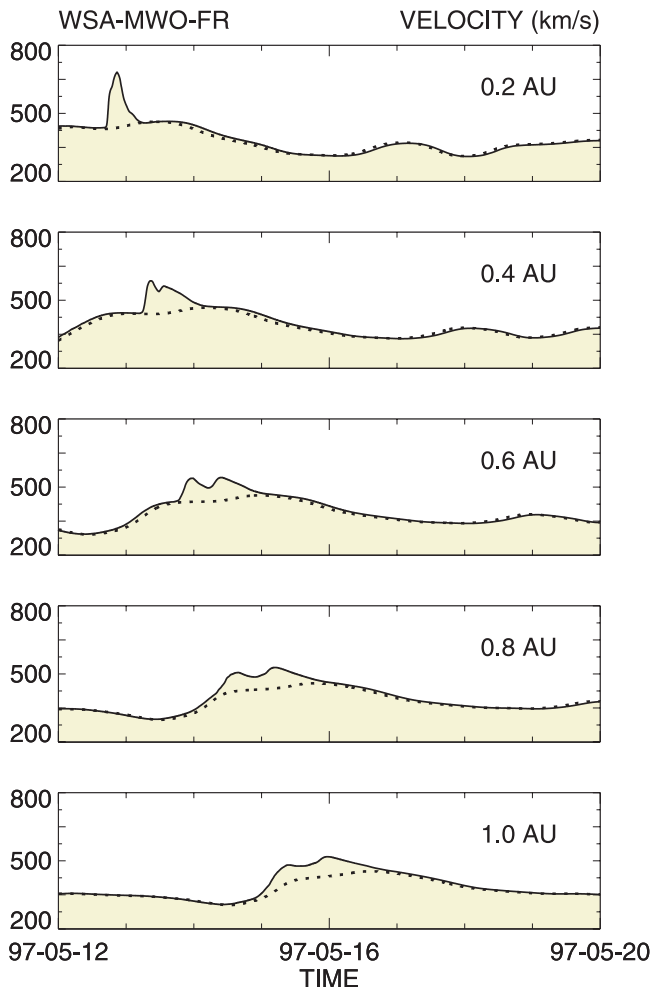

Figure 4. Evolution of the solar wind radial velocity at various points along the Sun-Earth line for computations with the background solar wind derived from the WSA-MWO-FR maps. The solid and dashed lines show results with and without the injection of the plasma cloud, respectively.

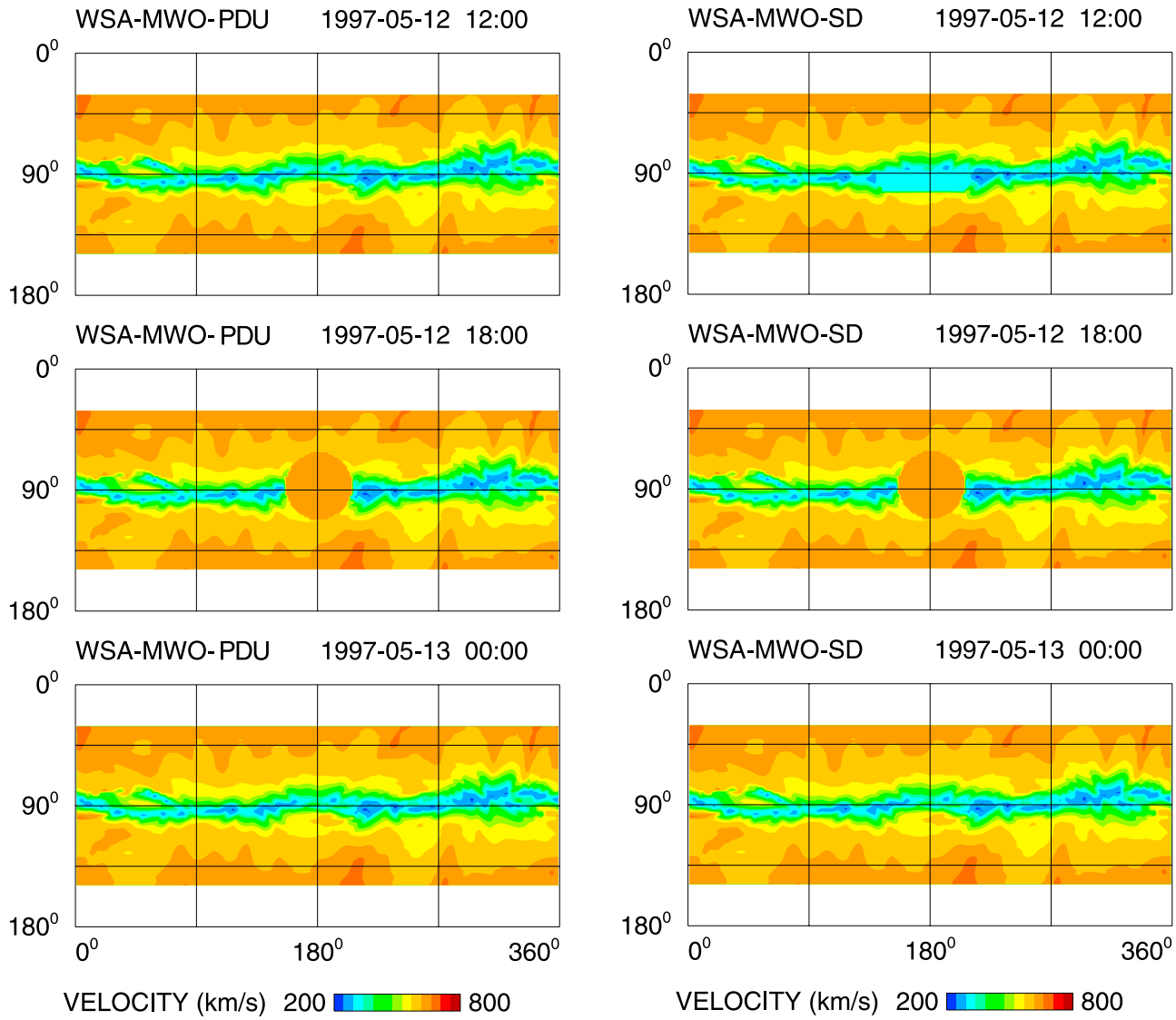

Figure 5. Distribution of the solar wind outflow velocity on the inner boundary (at 0.1 AU) at three different times for the (left) WSA-MWO pseudo daily updated (PDU) and (right) WSA-MWO "stream displacement" (SD) (see text) maps. The distribution of the radial velocity is shown (top) before, (middle) during, and (bottom) after the introduction of the input pulse.

and WSA model computations the shock merges with the CIR unless the fast flow from the southern excursion of the coronal hole is arbitrarily shifted east in longitude by more than 15°. This spatial shift roughly corresponds to 1.14 days and to the mean flow velocity of 152 km s^{-1} required for propagation between the solar surface and the inner boundary of the heliospheric model. This displacement is much larger than the uncertainties in the construction of the maps at the inner boundary. We therefore investigate the other possibility, which is whether the time dependence of the input flow structure needs to be accounted for in numerical simulations of the 12 May 1997 interplanetary event.

4.1. Pseudo Daily Updated Maps

[20] Figure 5 (left) shows the flow velocity at 21.5 R_S provided by the WSA-MWO model using WSA-MWO pseudo daily updated (PDU) photospheric magnetic field maps. We refer to the maps as pseudo daily updated to distinguish them from the traditional ones, which are constructed by adding the most recent magnetogram to the previous day's updated synoptic map (see *Arge and Pizzo* [2000] for a more complete description of daily updated and full rotation maps). These pseudo updated maps were constructed (using a technique similar to that used by *Zhao et al.* [1997]) from the Mount Wilson Carrington rotation (CR) maps 1921, 1922, and 1923 as follows. They were joined together end to end, and then 90 pseudo daily updated synoptic maps were constructed from them. The first map consisted of photospheric field data beginning at 180° longitude in CR 1922 (i.e., CR1922:180) and ending at CR1921:180. The next map began at CR1922:176 and ended at CR1921:176 and so on in 4° steps (i.e., the longitudinal resolution of the MWO maps). The first daily updated map was assigned an update time corresponding to the central meridian passage time of CR1922:000 (i.e., 180° in longitude from each end of the map). The other maps

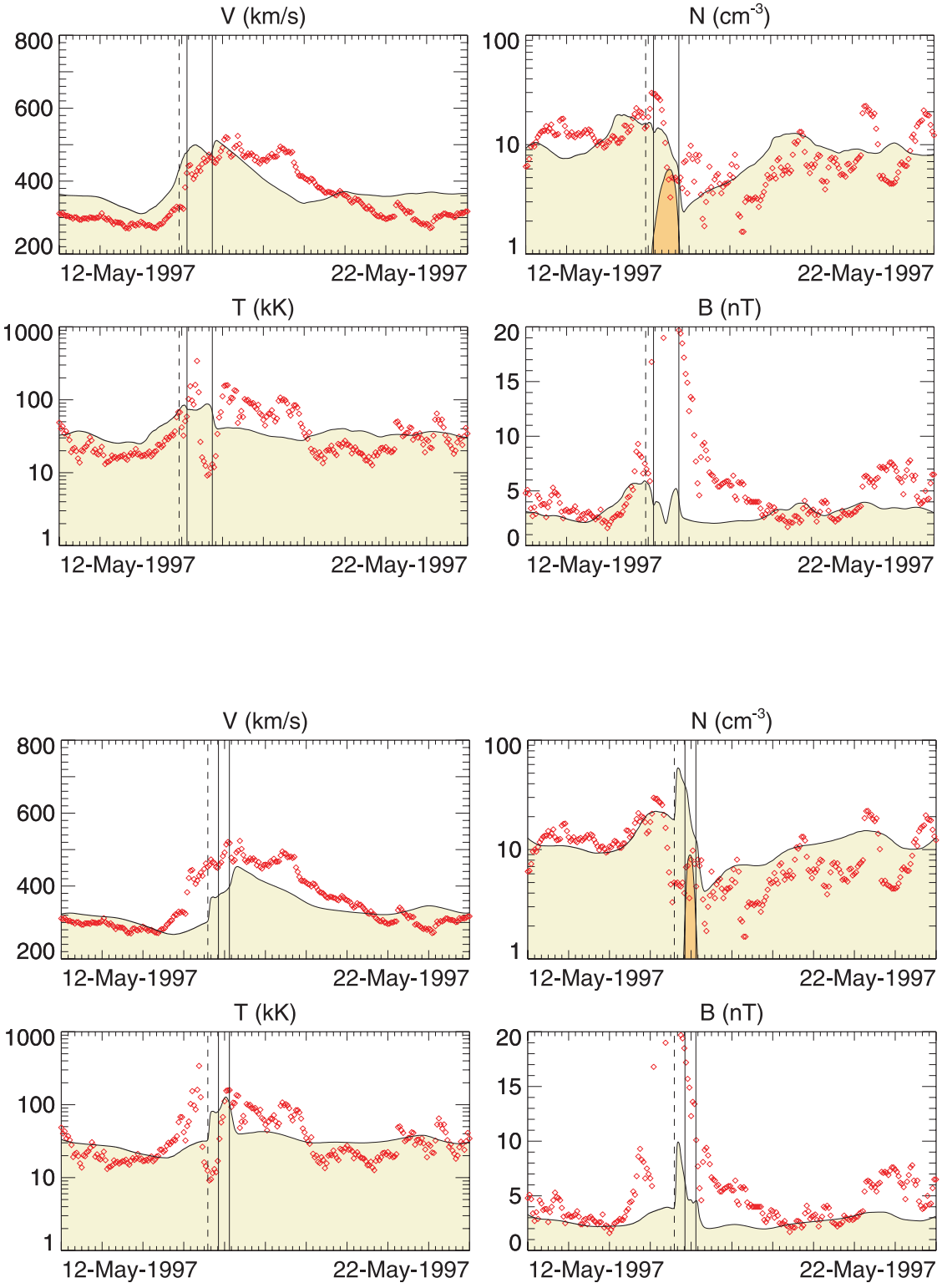

Figure 6. Evolution of solar wind parameters at Earth for the ICME propagating in the background solar wind derived from the (top) WSA-MWO-PDU and (bottom) WSA-MWO-SD maps. The visualization of parameters is the same as in Figure 2.

were assigned update times in a similar manner (i.e., the time when the middle of each map passed through the central meridian as viewed from Earth). The maps were thus "updated" approximately every one third of a day, and the seam, joining the two ends of the map, was positioned behind the Sun, as far away from the Sun-Earth line as possible. This minimizes the effects (in the earthward direction) of the discontinuity that occurs here. The other

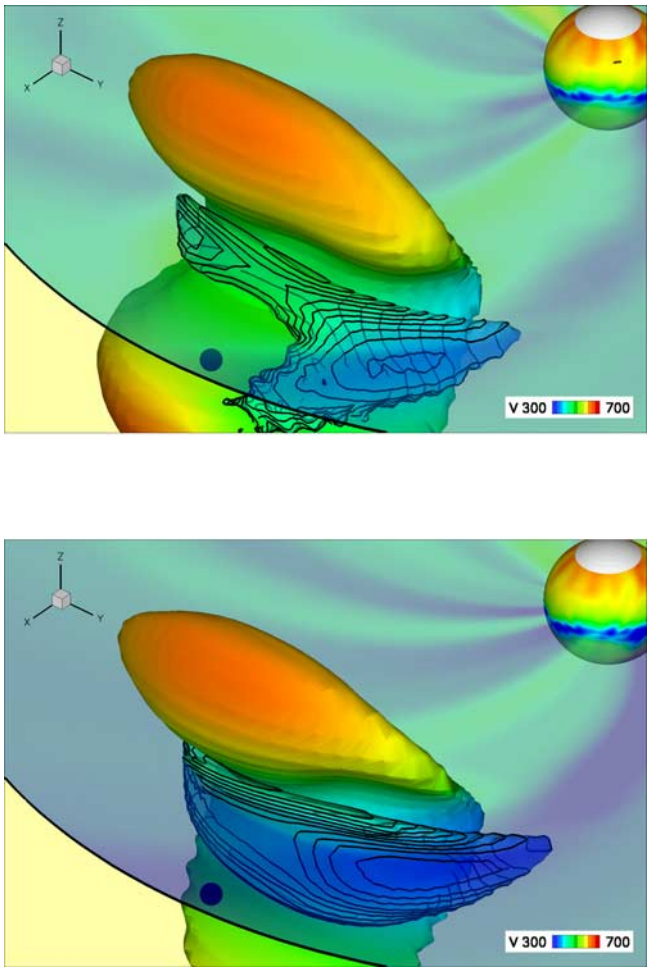

Figure 7. Visualization of an interplanetary disturbance on 15 May 1997 at 0000 UT for the ICME propagating in the background solar wind derived from the (top) WSA-KPNO-PDU and (bottom) WSA-MWO-SD maps. The visualization of parameters is the same as in Figure 3.

advantage to this approach is that the data used in these maps were from full rotation maps where each element on the map has been merged with all available observations made during a given Carrington rotation, especially those made near the central meridian. This minimizes problems at the poles where the photospheric field values are the least reliable and are thus prone to problems. The polar field in traditional daily updated maps can be problematic, especially near the leading edges of the maps, where the field values come from observations taken near the limb, far from the central meridian. A procedure was applied to CR maps 1921–1923 to both correct and fill (where necessary) the magnetic field measurements at the poles as described by *Arge and Pizzo* [2000].

[21] Figure 6 (top) shows the predicted evolution of plasma parameters at Earth together with the Wind spacecraft observations. It can be seen that the predicted temporal profiles are similar to those computed with the full rotation maps (Figure 2). This implies that the time-dependent variations in the solar wind parameters as derived from the photospheric magnetic field observations are not sufficient to modify noticeably large scale transient disturbances.

[22] Figure 7 (top) shows that the global heliospheric structures appear to be similar to those obtained with full rotation maps (see Figure 3). The merged CIR and shock can be identified, and this merging is seen also in Figure 8 (top). Note that small-amplitude modulations visible in the velocity profile at 0.2 and 0.4 AU smooth out at large heliocentric distances (see Figure 8, top).

4.2. Sudden Displacement of the Streamer

[23] On the basis of the previous unsatisfactory results we specify a scenario with much larger variations in the background solar wind structure. Namely, we mimic a sudden displacement of the streamer (or coronal hole boundary) that might happen after the coronal eruptive process. We assume that where there was a slow flow at the CME location prior to its launch, there is a fast flow following it.

[24] Figure 5 (right) shows the outflow velocity at the inner boundary at 21.5 R_S that we have artificially constructed from the WSA-MWO-FR maps. Figure 5 (middle) and Figure 5 (bottom) show the velocity structures during and after the CME launch, respectively (this is the same as in the WSA-MWO-FR scenario in Figure 2). Figure 5 (top) shows the velocity structure before the CME launch with our ad hoc modification. We have replaced fast stream values of the southern excursion of the coronal hole with mean values of the slow stream at the central meridian just below the equator. Thus we simulate a sudden northward displacement of the southern fast stream boundary and call this scenario WSA-MWO stream displacement (SD).

[25] Figure 6 (bottom) shows the predicted evolution of plasma parameters at Earth together with the Wind spacecraft observations. A qualitative difference from the previous WSA-MWO-FR (Figure 2) and WSA-MWO-PDU (Figure 6, top) cases can be seen. Now the interplanetary shock is well visible, with a clear standoff distance from the driving ejecta.

[26] Figure 7 (bottom) shows that while the global plasma cloud appears to be similar to those obtained with full rotation (Figure 3) or daily updated (Figure 7, top) maps, especially at high latitudes, the shock normal becomes perpendicular to the Sun-Earth line. This is due to the absence of the CIR ahead of the transient disturbance, and it is seen also in Figure 8 (bottom).

5. Comparison With Observations

[27] Solar wind parameters were observed by the Wind spacecraft upstream of Earth [*Webb et al.*, 2000]. An interplanetary shock arrived at Wind on 15 May at 0115 UT, followed later by the driving ejecta with an embedded magnetic cloud. Bidirectional electron flux was observed within the shocked plasma but not within the magnetic cloud [*Webb et al.*, 2000]. Suprathermal bidirectional electron flux and composition (unusual N_α/N_p ratio) signatures suggest that ejecta passage started earlier and lasted longer than estimated from solely magnetic cloud signatures [*Berdichevsky et al.*, 2002]. The Wind spacecraft exited the positive sector and (after triple crossing the sector boundary at 0038, 0518, and 0950 UT on 15 May) entered

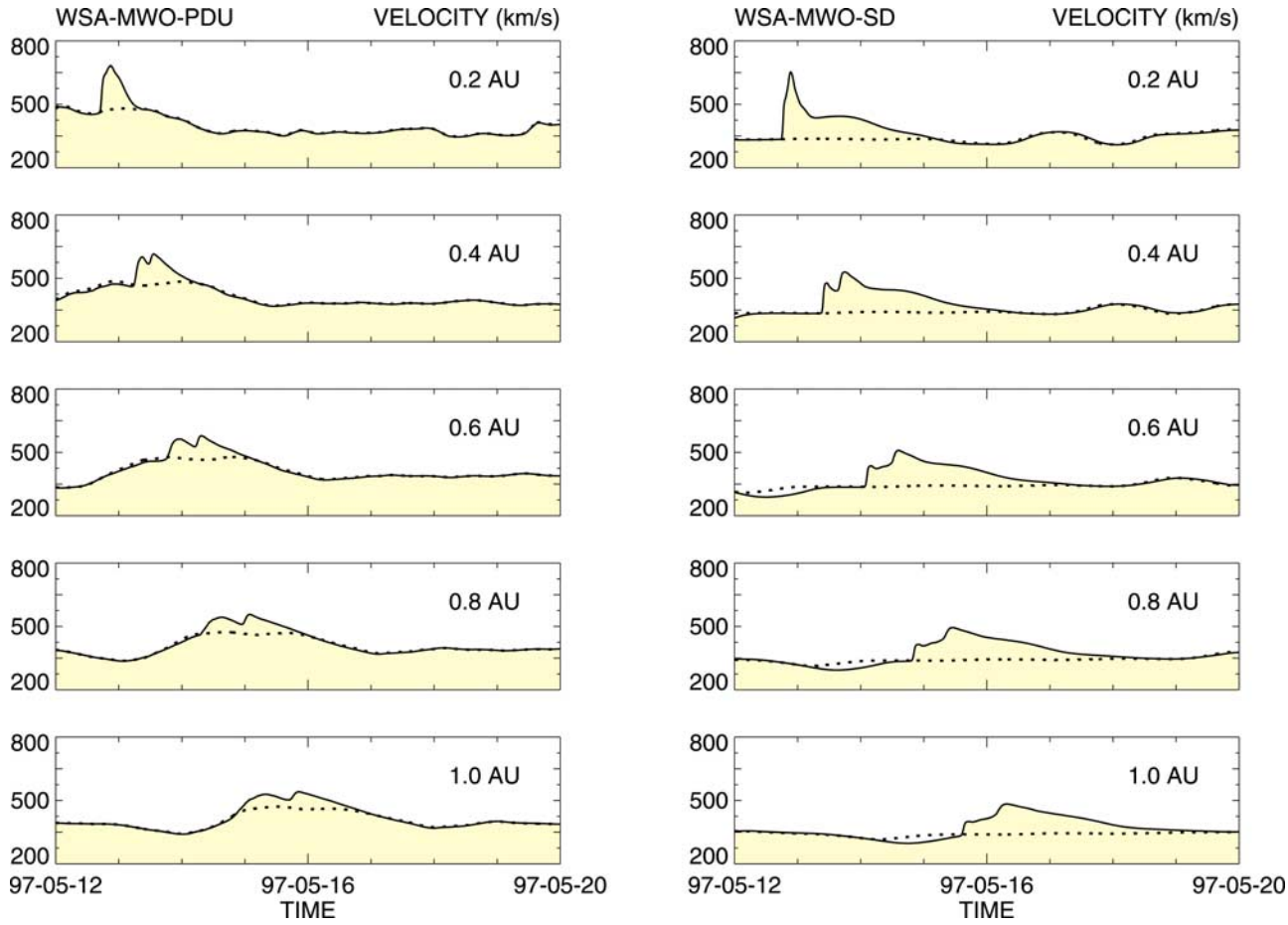

Figure 8. Evolution of the solar wind radial velocity at various points along the Sun-Earth line for computations with the background solar wind derived from the (left) WSA-MWO-PDU and (right) WSA-MWO-SD maps. The solid and dashed lines show results with and without the injection of the plasma cloud, respectively.

the magnetic cloud at 0951 UT [*Ivanov et al.*, 2003], and then, after exiting the cloud at 2330 UT on 15 May it was located mainly in the IMF negative sector until almost 0300 UT on 17 May. *Ivanov et al.* [2003] found that the high-speed flow from the low-latitude coronal hole also became involved in the interaction.

[28] Table 1 summarizes observed start and end times of the driving ejecta as fit by various techniques, together with ejecta signature duration and the standoff interval between the observed interplanetary shock and the leading edge of the ejecta. Table 2 lists the shock arrival times, inclinations of the shock normal, shock standoff interval, and ejecta duration as determined from observations and from our numerical computations. Large variations in ejecta fits make detail comparison with numerical simulations difficult.

Table 1. Start, End, and Duration of the Ejecta Signatures and the Shock Standoff Interval (Shock Arrival on 15 May 0115 UT) Observed at 1 AU

Signature	Start[a]	End[a]	Duration, hours	Standoff, hours:min	Reference
Magnetic cloud fit	15 May, 1000	16 May, 0100	15	8:45	*Webb et al.* [2000]
Magnetic cloud fit	15 May, 0900	16 May, 0100	16	7:45	*Watari et al.* [2001]
Magnetic cloud fit	15 May, 0951	15 May, 2350	14	8:36	*Ivanov et al.* [2003]
Magnetic cloud fit	15 May, 0900	16 May, 0200	17	7:45	*Lepping et al.* [2003]
Plasma signatures	15 May, 0950	–	–	8:35	*Webb et al.* [2000]
Large field rotation	15 May, 0900	15 May, 2400	15	7:45	*Berdichevsky et al.* [2002]
Strong magnetic field	15 May, 0500	15 May, 2400	19	3:45	*Berdichevsky et al.* [2002]
Strong magnetic field	16 May, 0600	16 May, 2400	–		
Low proton temperature	15 May, 0700	15 May, 2400	17	5:45	*Berdichevsky et al.* [2002]
Low plasma β	15 May, 1000	15 May, 2400	14	8:45	*Berdichevsky et al.* [2002]
Low plasma β	16 May, 0600	16 May, 1400	–		
$N_\alpha/N_p > 6\%$	15 May, 0500	16 May, 0300	22	3:45	*Berdichevsky et al.* [2002]
$N_\alpha/N_p > 6\%$	16 May, 0600	16 May, 1300	–		

[a]Times are in UT.

Table 2. Shock Arrival Time, Latitudinal (θ_N) and Longitudinal (φ_N) Inclination of the Shock Normal to the Sun-Earth Line, Shock Standoff Interval, and Ejecta Duration as Determined From Observations and From Numerical Computations

	Shock Arrival[a]	θ_N, deg	φ_N, deg	Standoff, hours:min	Duration
Berdichevsky et al. [2000][b]	15 May 0115	−19	28	–	–
Ivanov et al. [2003]	15 May, 0115	−16	27	8:36	14 hours
Computations with WSA-MWO-FR maps	15 May, 0336	55	30	2:58	12 hours, 56 min
Computations with WSA-MWO-PDU maps	14 May, 2230	65	25	5:31	14 hours, 53 min
Computations with WSA-MWO-SD maps	15 May, 1410	−3	0	6:13	6 hours, 25 min

[a]Times are in UT.
[b]See Table 1 for standoff and duration values.

[29] The numerical computations predict arrival of the shock very close to observations for all coronal maps used (see also Figures 2 and 6). About a 10-hour difference in the shock arrival times obtained using the WSA-MWO-FR and WSA-MWO-SD maps emphasizes the importance of the background solar wind parameters in propagation of transient disturbances.

[30] Predicting the shock normal is more challenging since its inclination to the Sun-Earth line depends on the initial parameters and relative positioning of the driver ejecta and ambient solar wind as well as on the subsequent dynamic interaction between the driver ejecta and structured solar wind. Table 2 shows that using the WSA-MWO-SD maps improves the match with observations in latitudinal inclination (θ_N, positive values are northward) but not in longitudinal inclination (φ_N, positive values are westward). These inclination angles differ because the shock merges with the leading edge of the moderate fast stream (WSA-MWO-FR and WSA-MWO-PDU maps) or it propagates into the slow stream (WSA-MWO-SD map).

[31] The ejecta in numerical computations is defined as the time during which the injected density is larger than 25% of its peak value. Note that launch of the driver ejecta at 21.5 R_S will produce short standoff shock distances because the formation of a shock and its separation from the driving ejecta below 21.5 R_S is neglected. Table 2 shows that using the WSA-MWO-SD map improves the match with the shock standoff interval but not with the ejecta duration. When the ICME is launched into the moderate fast stream (WSA-MWO-FR and WSA-MWO-PDU maps), the shock reaches its leading edge and decelerates while the ejecta expands in the moderate fast stream. This results in the shorter shock standoff intervals but the longer ejecta durations at 1 AU. When the ICME is launched into the slow stream and is followed by the fast stream (WSA-MWO-SD map), the ejecta is compressed, but the shock keeps its standoff distance. Note that *Odstrcil and Pizzo* [1999a] investigated similar but different interaction; a tilted slow streamer belt enabled a scenario in which both the ejecta and the shock were overtaken and compressed by the following fast stream.

[32] *Ivanov et al.* [2003] pointed out that the position of the forward shock relative to the leading boundary of the magnetic cloud does not agree completely with the *Berdichevsky et al.* [2000] assumption that it is a deflected wave undergoing quasi-stationary flow around the driving ejecta. Actually, the normals to the interplanetary shock and leading edge of the magnetic cloud diverge by $\approx 30^\circ$ and are directed southward and northward, respectively. *Ivanov et al.* [2003] suggested that this means that (1) the magnetic cloud turned to the south abruptly, (2) the shock changed its direction sharply while crossing the HCS, or (3) the magnetic cloud did not generate that shock. It is interesting to note that our computations with unmodified FR maps provide shocks with northward normals, i.e., the same as the observed magnetic cloud normals. This emphasizes the effect of background stream structure on transient disturbances.

6. Implications for Future in Situ and Remote Observations

[33] Obviously, single-point remote and in situ observations are insufficient to describe the event unambiguously and in detail since it is difficult to discern the three-dimensional, time-dependent structure. We have produced simulated temporal profiles of in situ observations and synthetic white light images to see how the different scenarios considered here might manifest themselves in STEREO observations. The In Situ Measurements of Particles and CME Transients (IMPACT) instruments will measure parameters of the IMF, solar wind plasma, and energetic particles. The heliospheric imagers will observe the Thomson scattering of the solar white light by interplanetary density structures.

6.1. Plasma Parameters

[34] The temporal evolution of plasma parameters has already been presented in Figures 2 and 6 as single-point observations at Earth. Multipoint in situ observations will provide a much better opportunity to deduce the 3-D structure of ambient and transient solar wind phenomena and to validate 3-D heliospheric models.

[35] Figure 9 shows our numerical simulations in the form of multipoint observations of the solar wind velocity at various observing positions leading and lagging Earth on the ecliptic at 1 AU. The WSA-MWO-FR (Figure 9, top) and WSA-MWO-SD (Figure 9, bottom) cases are shown, in which the ICME propagates into the background solar wind with and without a prior fast stream. These two cases produce different temporal profiles east of the Sun-Earth line (because of the presence or absence of the fast stream before the ICME launch) and similar temporal profiles west of the Sun-Earth line (where both cases have a slow stream).

[36] The ICME has been launched into the solar wind as a symmetric structure with respect to the Sun-Earth line. However, temporal profiles at 1 AU are not symmetric because of the corotating structured background solar wind. This effect is especially visible in the WSA-MWO-FR case (Figure 9, top) where the ICME propagates through the corotating fast stream resulting from the equatorward extension of the southern fast stream. This effect can also be

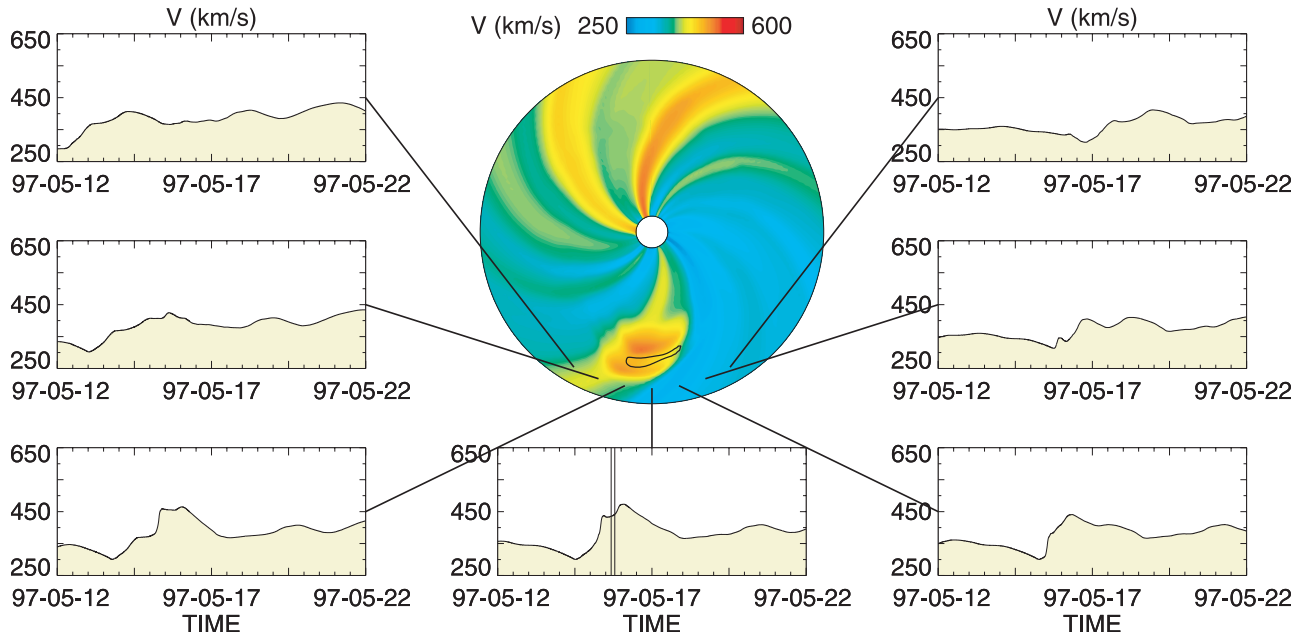

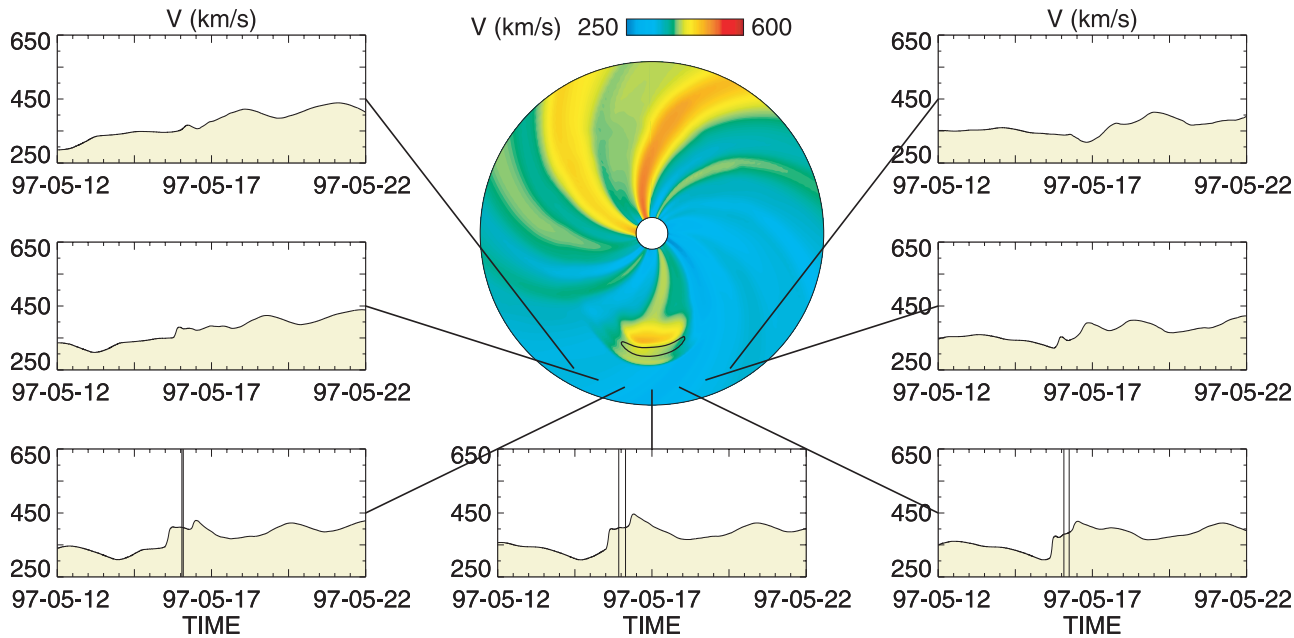

Figure 9. Simulated multipoint in situ observations of a transient disturbance at different positions in the equatorial plane at 1 AU shown for the (top) WSA-MWO-FR and (bottom) WSA-MWO-SD computations. The central circular images show a distribution of the solar wind radial velocity in the equatorial plane on 14 May 1997 at 1200 UT together with locations of the observing positions. The remaining plots show temporal evolution of the solar wind radial velocity at the observing positions located at 1 AU and at 150°, 160°, 170°, 180° (Earth), 190°, 200°, and 210° longitudes (counterclockwise from left), as indicated by solid lines. The vertical black solid lines indicate the extent of the injected density at 5 cm^{-3}, ~20–25% of its maximum value.

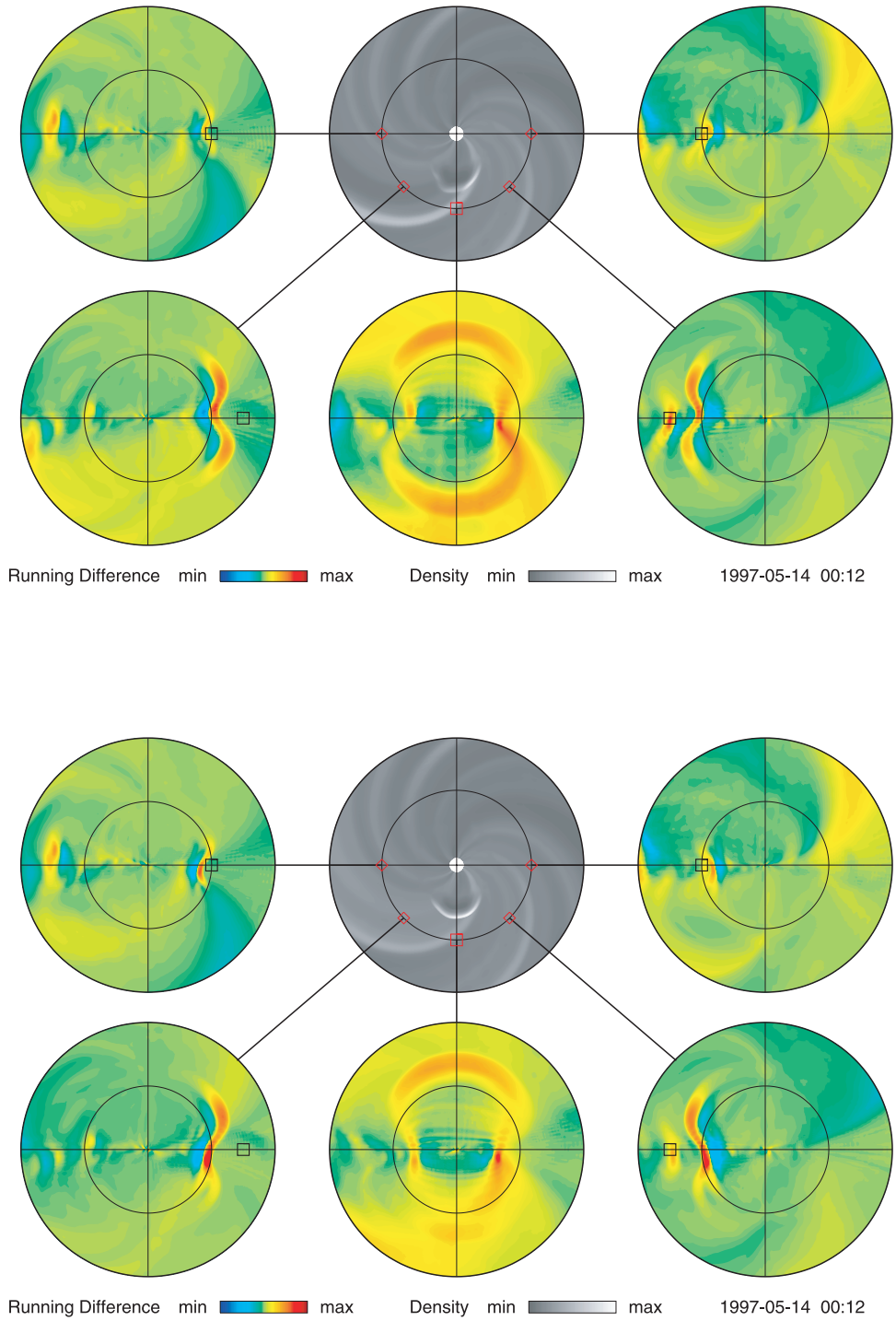

Figure 10. Simulated multiperspective remote observations of a transient disturbance from different positions in the equatorial plane at 1 AU are shown for the (top) WSA-MWO-FR and (bottom) WSA-MWO-SD computations. The middle top image (grey scale) in both panels shows the distribution of the solar wind density scaled by $(R_{AU}/r)^2$ in the equatorial plane on 14 May 1997 at 1200 UT together with locations of the observing positions. The inner and outer circles are at 1 and 1.7 AU, respectively. The remaining images show synthetic running difference images of the total white light brightness as viewed from the different 1-AU observing positions at 90°, 135°, 180° (Earth), 225°, and 270° longitudes (counterclockwise from left), as indicated by solid lines. The running difference images correspond to 1200 and 0600 UT on 14 May. For each running difference view the Sun is at center, and the inner and outer circles are at 45° and 90° elongation, respectively. The Earth's position is shown by the black square.

seen in the WSA-MWO-SD (Figure 9, bottom) where the ICME propagates just above the fast stream stemming from the southern coronal hole. Despite interactions with the structured background solar wind the ICME maintains roughly its original azimuthal extent. Note that the extent of the ejected material is less than the extent of the interplanetary shock driven by the ejecta. Thus each spacecraft may observe very different plasma properties.

[37] Temporal profiles are different at each observing point along the ecliptic plane at 1 AU (Figure 9): Almost undisturbed background solar wind is observed at ±30°, an interplanetary shock is observed at ±20°, and an interplanetary shock followed by the ICME is observed at smaller separations. At +20° (−20°) the interplanetary shock is propagating in a fast (slow) stream east (west) from the Sun-Earth line. At Earth the interplanetary shock is merged with the leading edge of the corotating fast stream. In the WSA-MWO-FR case (Figure 9, top) the ICME is azimuthally distorted, and its speed is greater because of the parameters of the background solar wind.

[38] Note that knowledge of the solar wind velocity east of the Sun-Earth line (i.e., observations from a spacecraft behind the Earth) can be used (1) to predict the arrival of recurrent fast streams, (2) to improve estimates of ICME propagation times in empirical models, and (3) to provide warning on possible compound events (CIRs followed by ICMEs) that are usually more geoeffective than ICME-only events [*Burlaga et al.*, 1987; *Tsurutani et al.*, 1999].

6.2. Synthetic Images

[39] Multiperspective remote observations will provide an unprecedented opportunity to track interplanetary disturbances. To investigate the likely appearance of heliospheric white light structures from several viewpoints, we take line-of-sight (LOS) integrals [*Hundhausen*, 1993] through the 3-D density distribution provided by the heliospheric MHD model. Note that instrumental noise, the zodiacal light background, and other complications are not considered in our synthetic images, so our structures show more contrast than will be observed.

[40] The total brightness images have very low contrast, and careful postprocessing is needed to enhance the visibility of ambient structures and transient disturbances. The running difference technique shows transient structures best, and it is effective even in cases having highly inhomogeneous solar wind background structures. Note that we use a 6-hour interval between successive images, i.e., a much slower cadence than is typically used in coronagraph imaging. This is because the ICMEs and associated shock-compressed densities expand slowly on the large spatial scale associated with interplanetary disturbances.

[41] Figure 10 shows synthetic images generated from the 3-D density distribution as they might be observed from five vantage points at 1 AU. The running difference between images generated at 1200 and 0600 UT on 14 May is depicted. It is possible to identify the main morphology of the ICME, although the initial enhancement of the simulated ICME was relatively moderate. Note that changes in structures near the observer are more evident than changes in more remote ones. The front view shows the ICME as a ring of enhanced brightness encircling the Sun. The ICME halo is brighter to the north than to the south; a similar behavior has been observed in coronal imagery for the 12 May 1997 event [*Plunkett et al.*, 1998]. Note that the CIR can be visible as well, especially in cases of transverse propagation with respect to the observer. The differencing emphasizes the structure of the ICME that becomes strongly affected by its interaction with the structured solar wind. The largest compression occurs at the slow dense streamer belt and leads to the formation of an arc-like density structure (see Figures 3 and 7). This compression appears as two bright spots in the LOS integration (see *Tokumaru et al.* [2003] for observation of a strong ICME using interplanetary scintillation). The side views show the latitudinally distorted shape of the ICME, and the effect of the preceeding CIR on the ICME shape can be seen. Note the differing inclinations of the leading edge of the ICME with respect to the equatorial plane; the inclination is northward (southward) for the ICME propagating in a solar wind with (without) a preceeding fast stream.

7. Discussion and Conclusion

[42] We have applied the 3-D MHD numerical model to the 12 May 1997 interplanetary event to analyze possible interactions of the ICME propagating in various steady state and evolving configurations of the background solar wind. This work is similar to paper 1, which uses the SAIC coronal model and Kitt Peak National Observatory magnetograms, but instead, this work uses the WSA coronal model and Mount Wilson Observatory magnetograms. In addition to the full rotation maps we have also used pseudo daily updated maps and artificially modified maps to simulate the temporal variation of the ambient solar wind and rapid displacement of the streamer boundary, respectively. Initial parameters of the ICME, derived from the cone model of the SOHO/LASCO observations, were the same in both works except for adjustments needed to account for the different locations of the model inner boundary and for specifying the input pulse as a spherical cloud passing through the inner boundary in this work. It is an appealing characteristic of "data-inspired" (in contrast to "data-driven") models that one can vary key parameters of the ambient and transient features to assess the consequences and thus to acquire a deeper understanding of the physics involved.

[43] Using different coronal input maps, we have confirmed our main conclusions previously presented in paper 1: (1) It is becoming ever more feasible to simulate large-scale structures and parameters of the ambient solar wind and to estimate the arrival of interplanetary shocks and coronal ejecta, and (2) small-scale solar wind structures can significantly affect the appearance of transient disturbances. Further, detailed analysis of the 12 May 1997 heliospheric simulations presented in this paper shows that (1) shock inclination and separation from the ejecta cannot be fully matched by using the full rotation source-surface maps, (2) using daily updated photospheric observations does not provide enough variations in the background solar wind to improve match with observations (observations at 1 R_S are not sufficient to reproduce changes in the coronal flow structure caused by a CME launch), and (3) it is necessary to modify the flow topology by the sudden displacement of the southern coronal hole boundary or by the emergence of

a post-CME fast flow (eruption flow lasts longer than the flux rope). Finally, we have also produced simulated multipoint in situ temporal observations and multiperspective remote synthetic white light images to see how different scenarios may manifest themselves in future observations.

[44] The overall global ambient solar wind structure matches observations at 1 AU very well for both SAIC and WSA coronal models. The latitudinal excursion of the southern coronal hole near the central meridian in the SAIC coronal model produces faster flow than does the WSA coronal model. However, the treatment of smaller-scale features and the time dependency need further sophistication in both models. *Fainshtein and Kaigorodov* [1994] found that the divergence of the magnetic flux tube from a coronal hole depends not only on the area of the hole but also on the radial magnetic field intensity at its base. These authors also detected a positive correlation at the Earth's orbit between the velocity of the associated high-speed solar wind and the radial component of the magnetic field in the stream. Neither the WSA nor SAIC model accounts for the above effect.

[45] Further, *Zhao and Hoeksema* [1996] found that virtually no significant changes in the location of the coronal streamer belt at the HCS are observed after CME launch. This implies a certain insensitivity of the photospheric magnetic field to CME launch and suggests that the preexisting helmet structure may reform on relatively short timescales. Since both the SAIC and WSA coronal models are based on photospheric observations, they cannot properly resolve eventual temporal variations of the coronal structures at 30 and 21.5 R_S during and after large-scale eruptive processes, respectively.

[46] We have assumed that an ejected plasma cloud with diameter, speed, and direction determined by the cone model should constitute a reasonable approximation for the interplanetary shock driver in the simulations. Recently, *Stockton-Chalk* [2002] presented a statistical study of the nonradial expansion of 50 CMEs seen beyond a few solar radii off the solar limb with SOHO/LASCO between 1997 and 2000, and the extent of the latitudinal expansion is, on average, only 1.84°. This supports the key assumption in the cone model, constant angular extent, used to derive the geometrical and kinematic parameters of the observed CME [*Zhao et al.*, 2002]. Thus the main problem with the cone model is the uncertainty in fitting the diffuse periphery of the halo CME. Future multiperspective observations by the STEREO spacecraft will provide significant improvement in detection and fitting of CMEs.

[47] It is well established that purely hydrodynamic model ejecta lead to large distortions of simulated ICMEs propagating in an ambient medium with a realistic large-scale velocity structure [e.g., *Odstrcil and Pizzo*, 1999a, 1999b]. For ICMEs with an embedded magnetic structure it is anticipated that tension in the field lines will reduce but not eliminate the distortion [see *Schmidt and Cargill*, 2001]. Hence the lack of any information on the magnetic structure of the CME from the cone model should not affect the overall dynamics to any great degree. Nevertheless, the absence of internal magnetic structure within the model ICMEs is a drawback that affects the distribution of thermal and magnetic pressures (and hence densities and temperatures within ICMEs) as well as the connectivity of certain IMF lines. However, more accurate CME models directly driven by photospheric observations are currently under development.

[48] A number of studies suggest that temporal variations in the solar corona may follow large eruptions and they can cause the displacement of the fast stream boundary or a sudden opening of the coronal hole. *Pizzo* [1983] showed an example of substructures with amplitudes of 100 km s^{-1} which come and go, and the shape and location of the stream fronts shift back and forth on periods of several hours to a day between 0.3 and 1 AU as observed by Helios spacecraft. *Harvey et al.* [1986] found changes in Helium I synoptic maps of coronal holes associated with filament eruptions (coronal holes either enlarged or formed) and speculated that transient high-speed solar wind streams may occur in association with these transient coronal hole changes. *Kaigorodov and Fainshtein* [1991] detected fast variations (with a typical timescale <24 hours) in the area of foot points, and they identified seven cases of such variations for CR maps 1680–1682 with corresponding changes in the flow velocity of ~20 km s^{-1} at Earth. *Bravo* [1995] suggested a scenario in which nearby coronal holes play an important role in solar eruptive phenomena and topological changes of coronal holes lead to fast solar wind flow. Our numerical computations suggest that such a scenario might have occurred during and after the 12 May 1997 solar eruptive event. However, there is no direct observational evidence to confirm this suggestion, since posteruptive effects are hidden behind a halo CME. Such effects could be detected by multipoint and multiperspective observations like those anticipated by the STEREO spacecraft.

[49] The present study suggests that high-quality solar observations can be used to predict the basic features of subsequent interplanetary disturbances. However, additional work is necessary to specify finer-scale structures, more accurate locations, and the temporal evolution of the stream boundaries in the corona. Numerical heliospheric MHD models on supercomputers are reaching a point where current photospheric and coronal observations have become a limitation. New observations, especially at greater coronal heights, and multiperspective imaging are inevitable for reliable, accurate, and detailed specification of ambient and transient structures in the heliosphere. Of course, continuing development of numerical models (both in improving numerical resolution and in including more detailed physics) is to be pushed forward. Finally, we would like to note that when new phenomena and effects are investigated, it is always an advantage to use different models for the same problem. Not only can one obtain higher confidence in predicted features and effects, but also the differences in results are very helpful in estimating their accuracy, in understanding the physics, and in learning what should be improved in the future.

[50] **Acknowledgments.** This work has been supported by the DoD-AFOSR/MURI (Multi-Disciplinary Research Initiative) and NSF/CISM (Center for Integrated Space Weather Modeling) projects. Additional support was from NSF/SHINE program and grants A3003003 and S10030067 from the Academy of Sciences and Grant Agency of the Czech Republic. Computational facilities were provided by National Center for Atmospheric Research in Boulder, Colorado. We acknowledge data from Mount Wilson Solar Observatory, ESA-NASA SOHO/LASCO project, and the NASA National Space Science Data Center. We thank Doug Biesecker for reviewing the manuscript.

[51] Shadia Rifai Habbal thanks Eugene P. Romashets and J. Americo Gonzalez-Esparza for their assistance in evaluating this paper.

References

Arge, C. N., and V. J. Pizzo (2000), Improvement in the prediction of solar wind conditions using near-real time solar magnetic field updates, *J. Geophys. Res.*, *105*, 10,465–10,480.

Arge, C. N., D. Odstrcil, V. J. Pizzo, and L. Mayer (2002), Improved method for specifying solar wind speed near the Sun, in *Solar Wind Ten*, edited by M. Velli and R. Bruno, *AIP Conf. Proc.*, *679*, 190–193.

Arge, C. N., J. G. Luhmann, D. Odstrcil, C. J. Schrijver, and Y. Li (2004), Stream structure and coronal sources of the solar wind during the May 12th, 1997 CME, *J. Atmos. Sol. Terr. Phys.*, *66*, 1295–1309.

Berdichevsky, D. B., A. Szabo, R. P. Lepping, A. F. Vinas, and F. Mariani (2000), Interplanetary fast shocks and associated drivers observed through the 23rd solar minimum by Wind over its first 2.5 years, *J. Geophys. Res.*, *105*, 27,289–27,314.

Berdichevsky, D. B., C. J. Farrugia, B. J. Thompson, R. P. Lepping, D. V. Reames, M. L. Kaiser, J. T. Steinberg, S. P. Plunkett, and D. J. Michels (2002), Halo-coronal mass ejections near the 23rd solar minimum: Lift-off, inner heliosphere, and in situ (1 AU) signatures, *Ann. Geophys.*, *20*, 891–916.

Bravo, S. (1995), A solar scenario for the associated occurrence of flares, eruptive prominences, coronal mass ejections, coronal holes, and interplanetary shocks, *Sol. Phys.*, *161*, 57–65.

Burlaga, L. F., K. W. Behannon, and L. W. Klein (1987), Compound streams, magnetic clouds, and major geomagnetic storms, *J. Geophys. Res.*, *92*, 5725–5734.

Fainshtein, V. G., and A. P. Kaigorodov (1994), On a possible control mechanism for solar wind outflow velocity from coronal holes, *Sol. Phys.*, *152*, 429–444.

Harvey, K. L., N. R. Sheeley Jr., and J. W. Harvey (1986), HE I 1083 A observations of two-ribbon flare-like events associated with filament disappearances, paper presented at Solar-Terrestrial Predictions Workshop, Natl. Oceanic and Atmos. Admin., Meudon, France.

Hundhausen, A. J. (1993), Size and locations of coronal mass ejections: SMM observations from 1980 and 1984–1989, *J. Geophys. Res.*, *98*, 13,177–13,200.

Ivanov, K. G., A. V. Belov, A. F. Kharshiladze, E. P. Romashets, V. Bothmer, P. J. Cargill, and I. S. Veselovsky (2003), Slow dynamics of photospheric regions of the open magnetic field of the Sun, solar activity phenomena, substructure of the interplanetary medium and near-Earth disturbances of the early 23rd cycle: March–June 1997 events, *Int. J. Geomagn. Aeron.*, *4*, 91–109.

Kaigorodov, A. P., and V. G. Fainshtein (1991), Diurnal variations of open magnetic tubes from coronal holes and the neutral line on the source surface and related effects in the solar wind, *Adv. Space Res.*, *11*(1), 51–56.

Lepping, R. P., D. B. Berdichevsky, A. Szabo, C. Arqueros, and A. J. Lazarus (2003), Profile of an average magnetic cloud at 1 AU for the quiet solar phase: Wind observations, *Sol. Phys.*, *212*, 425–444.

Odstrcil, D., and V. J. Pizzo (1999a), Three-dimensional propagation of coronal mass ejections (CMEs) in a structured solar wind flow: 1. CME launched within the streamer belt, *J. Geophys. Res.*, *104*, 483–492.

Odstrcil, D., and V. J. Pizzo (1999b), Distortion of interplanetary magnetic field by three-dimensional propagation of CMEs in a structured solar wind flow, *J. Geophys. Res.*, *104*, 28,225–28,239.

Odstrcil, D., P. Riley, J. A. Linker, R. Lionello, Z. Mikic, and V. J. Pizzo (2003), 3-D simulations of ICMEs by coupled coronal and heliospheric models, in *Proceedings of International Solar Cycle Studies 2003: Solar Variability as Input to the Earth's Environment*, *Eur. Space Agency Spec. Publ., ESA-SP 535*, 541–546.

Odstrcil, D., P. Riley, and X. P. Zhao (2004), Numerical simulation of the 12 May 1997 interplanetary CME event, *J. Geophys. Res.*, *109*, A02116, doi:10.1029/2003JA010135.

Pizzo, V. J. (1983), Quasi-steady solar wind dynamics, in *Solar Wind Five*, edited by M. Neugebauer, *NASA Conf. Publ., CP-2280*, 675–691.

Plunkett, S. P., B. J. Thompson, R. A. Howard, D. J. Michels, O. C. St. Cyr, S. J. Tappin, R. Schwenn, and R. L. Lamy (1998), LASCO observations of an Earth-directed coronal mass ejection on May 12, 1997, *Geophys. Res. Lett.*, *25*, 2477–2480.

Riley, P., J. A. Linker, and Z. Mikic (2001), An empirically-driven global MHD model of the solar corona and inner heliosphere, *J. Geophys. Res.*, *106*, 15,889–15,901.

Schatten, K. H. (1971), Current sheet magnetic model for the solar corona, *Cosmic Electrodyn.*, *2*, 232–245.

Schmidt, J. M., and P. J. Cargill (2001), Magnetic cloud evolution in a two-speed solar wind, *J. Geophys. Res.*, *106*, 8283–8289.

Stockton-Chalk, A. (2002), The limit of non-radial expansion of coronal mass ejections, in *Proceedings of the Second Solar Cycle and Space Weather Euroconference*, *Eur. Space Agency Spec. Publ., ESA-SP 477*, 277–280.

Tokumaru, M., M. Kojima, K. Fujiki, M. Yamashita, and A. Yokobe (2003), Toroidal-shaped interplanetary disturbance associated with the halo coronal mass ejection event on 14 July 2000, *J. Geophys. Res.*, *108*(A5), 1220, doi:10.1029/2002JA009574.

Tsurutani, B. T., Y. Kamide, J. K. Arballo, W. D. Gonzales, and R. P. Lepping (1999), Interplanetary causes of great and superintense magnetic storms, *Phys. Chem. Earth, Part C*, *24*, 101–105.

Wang, Y. M., and N. R. Sheeley Jr. (1995), Solar implications of Ulysses interplanetary field measurements, *Astrophys. J.*, *447*, L143–L146.

Watari, S., T. Watanabe, and K. Marubashi (2001), Soft X-ray solar activities associated with interplanetary magnetic flux ropes, *Sol. Phys.*, *202*, 363–384.

Webb, D. F., R. P. Lepping, L. F. Burlaga, C. E. DeForest, D. E. Larson, S. F. Martin, S. P. Plunkett, and D. M. Rust (2000), The origin and development of the May 1997 magnetic clouds, *J. Geophys. Res.*, *105*, 27,251–27,259.

Zhao, X. P., and J. T. Hoeksema (1996), Effect of coronal mass ejections on the structure of the heliospheric current sheet, *J. Geophys. Res.*, *101*, 4825–4834.

Zhao, X. P., J. T. Hoeksema, and P. H. Scherrer (1997), Modeling boot-shaped coronal holes using SOHO-MIDI magnetic measurements, in *Proceedings of Fifth SOHO Workshop*, *Eur. Space Agency Spec. Publ., ESA-SP 404*, 751–755.

Zhao, X. P., S. P. Plunkett, and W. Liu (2002), Determination of geometrical and kinematical properties of halo coronal mass ejections using the cone model, *J. Geophys. Res.*, *107*(A8), 1223, doi:10.1029/2001JA009143.

N. Arge, Space Vehicles Directorate, Air Force Research Laboratory, Hanscom AFB, MA 01731-3010, USA. (nick.arge@hanscom.af.mil)

D. Odstrcil and V. Pizzo, Space Environment Center, NOAA, 325 Broadway, Boulder, CO 80305, USA. (dusan.odstrcil@noaa.gov; vic.pizzo@noaa.gov)